High Optical Absorption of Indium Sulfide Nanorod Arrays Formed by Glancing Angle Deposition

Mehmet F. Cansizoglu,[†,*] Robert Engelken,[‡] Hye-Won Seo,[§] and Tansel Karabacak[†]

[†]Department of Applied Science, University of Arkansas at Little Rock, Little Rock, Arkansas 72204, [‡]Electrical Engineering Program, Arkansas State University, State University (Jonesboro), Arkansas 72467, and [§]Department of Physics and Astronomy, University of Arkansas at Little Rock, Little Rock, Arkansas 72204

ABSTRACT Indium(III) sulfide has recently attracted much attention due to its potential in optical sensors as a photoconducting material and in photovoltaic applications as a wide band gap material. On the other hand, optical absorption properties are key parameters in developing photosensitive photodetectors and efficient solar cells. In this work, we show that indium sulfide nanorod arrays produced by the glancing angle deposition technique have superior absorption and low reflectance properties compared to conventional flat thin film counterparts. We observed an optical absorption value of approximately 96% for nanorods at wavelengths <500 nm in contrast to 79% for conventional thin films of indium sulfide. A superior photoconductivity (PC) response as high as about 40% (change in resistance upon illumination) was also observed in nanorod samples. This is mainly believed to be due to their high optical absorption, whereas only less than 1% PC change was detected in conventional thin films. We give a preliminary description of the enhanced light absorption properties of the nanorods by using the Shirley—George model, which predicts diffusion of light as a function of the roughness of the surface.

KEYWORDS: indium sulfide · nanorods · glancing angle deposition · GLAD · oblique angle deposition · light absorption · optical absorption · photoconductivity

Indium(III) sulfide (In_2S_3) (hereby referred to simply as indium sulfide) has promising properties for photovoltaic and optoelectronic device applications due to its relatively wide band gap, large photosensitivity and photoconductivity,[1−3] and stable chemical composition and physical characteristics at ambient conditions.[2−5] Indium sulfide exists in a defect spinel β-In_2S_3 form at room temperature.[4,5] It is intrinsically an n-type[6,7] semiconductor. Its band gap is reported to be between 1.9 and 3.3 eV, with most reported values in the vicinity of 2.0 eV,[1,12,15] but there is still controversy on whether it is a direct[8,9] or indirect[10,11] band gap material. Besides its promising optoelectronic characteristics, from an environmental point of view, it is free of highly toxic heavy metals, unlike CdS, CdSe, and CdTe, which are popular in solar cell applications.[15−18] Furthermore, the solar conversion efficiencies in solar cells with indium sulfide layers have recently been reported as high as 18.1%.[19,20]

Various synthesis methods for indium sulfide, for example, chemical vapor deposition (CVD),[15] chemical bath deposition, chemical transport reaction,[1] sputtering,[15] spray pyrolysis,[13,14] and thermal evaporation,[13,14] were adopted by different groups. Most of the previous studies on indium sulfide have focused on the effects of crystal structure, effects of doping, annealing, and stoichiometry,[2,1,3,12,15,16,20] but there have been limited studies on the effects of nanostructuring on optical and electrical characteristics of indium sulfide.[21−25]

Nanorod arrays have recently attracted much attention due to their unusually high levels of optical absorption[23,28] and superior electrical[26] and magnetic[27] properties. One critical issue is creating high optical absorbance materials,[28] which is a vital factor in photonic applications such as photovoltaics and optical sensors. Previously, various groups utilized surface textured morphologies in order to decrease the index of refraction and enhance the antireflection, thus increasing trapping of light within the thin film layer, using methods such as anisotropic etching, lithography techniques,[28−31] and glancing angle deposition (GLAD).[32,33]

In this study, we mainly focused on the effect of nanorod morphology on the light absorbance, transmittance, and reflectance characteristics of In_2S_3 materials. We show that, by utilizing a nanorod morphology produced by GLAD, it is possible to achieve a significant increase in the absorbance compared to conventional flat thin films. We explain this through an enhanced random multiple scattering caused by strong diffusion of light. In addition, the significant enhancement in the photoconductivity of nanorods is also believed to be due, in part,

*Address correspondence to mfcansizoglu@ualr.edu.

Received for review September 8, 2009 and accepted January 19, 2010.

Published online February 4, 2010.
10.1021/nn901180x

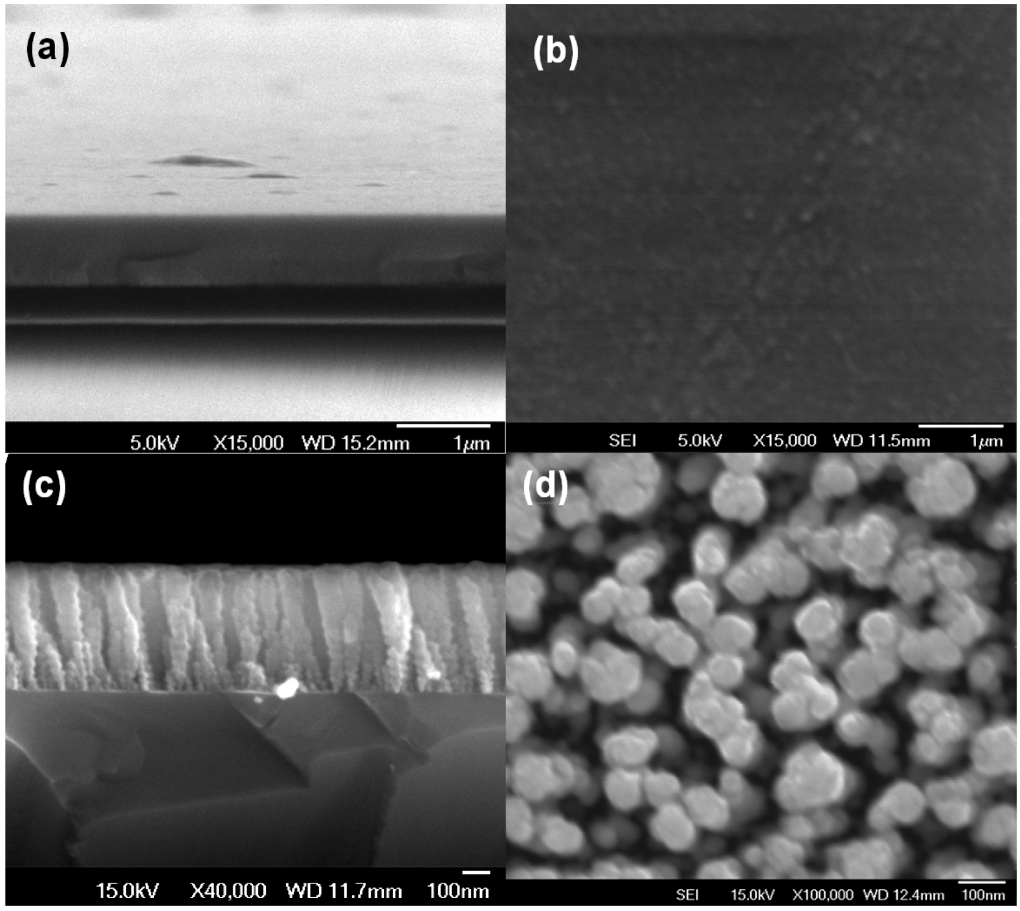

Figure 1. (a) Cross section and (b) top view SEM images of the normal incidence-deposited indium sulfide thin film with a thickness of 730 nm grown on a glass substrate, (c) cross section and (d) top view SEM images of 550 nm indium sulfide nanorod arrays grown by glancing angle deposition (GLAD) on a glass substrate are shown. The scale bars are 1 μm for the thin film and 100 nm for the 550 nm long nanorods.

to the larger optical absorption of the nanostructured material.

RESULTS AND DISCUSSION

In Figure 1a,b, are shown the cross section and top views of SEM images of the 730 nm thick thin film of indium sulfide, respectively. The sample was deposited using conventional normal incidence evaporation. A continuous and slightly rough surface morphology is observable on the film surface. The cracks observed on the cross-section image are due to mechanical cleaving during the sample preparation.

Cross section and top view SEM images of GLAD-deposited indium sulfide nanorod sample with a length of 550 nm are shown in Figure 1c,d. As can be seen in the SEM images, nanorod arrays are vertically aligned on the substrate. The helical structure observed on the cross section nanorod image (Figure 1c) is due to the slow axial rotation speed during deposition. The porosity of the 550 nm long nanorods (defined as the ratio of the volume of the gaps between the rods to the total volume of gaps plus rods) was calculated to be approximately 31.1% by image analysis on SEM pictures using a commercial computer software package (SPIP). The nanorod diameter was measured to be approximately 125 nm. EDAX analysis indicated that atomic percentages of In and S were approximately 41.1% and 58.7%, respectively, and are close to the ideal 2/3 stoichiometric ratio in In_2S_3.

Optical measurements included total (specular plus diffuse) reflectance (R), transmittance (T), and percentage absorption (A) spectra of indium sulfide samples deposited on glass. Reflectance and transmittance data are given as the percentage ratios of reflected and transmitted light to the incident light, respectively, and percentage absorption is calculated as $A = 1 - T - R$. The results are plotted in Figure 2a−c for T, R, and A, respectively. All of these figures display significant differences in their optical response between thin film and nanorod morphologies. In Figure 2a, nanorods exhibit a considerably smaller reflectance compared to the thin film. Within the window of 300 to 800 nm, the reflectance of a thin film with a thickness of 730 nm was measured to be approximately 20%. Between 600 and 800 nm, reflectance fluctuates around 20% due to interference effects from the surface.[12,34] In the range of wavelengths larger than 800 nm, the interference effect and, thus, fluctuation become more significant. On the other hand, for nanorod samples, the reflectance decreases down to as little as 3%, especially for longer nanorods (550 nm). The reflectance is inversely proportional to the length of the samples: approximately 5% for 495 nm and 7% for 220 nm. The sharp oscillations between 800 to 900 nm are due to a detector shift by the instrument at this point.

As can be seen in Figure 2b, the transmittance for 220 nm long nanorods at the 400 nm wavelength is less than 20%, where it is below 3% for 550 nm long nanorods. This can be partly attributed to the increased material volume and, therefore, increased penetration path for longer nanorods. The decrease in transmit-

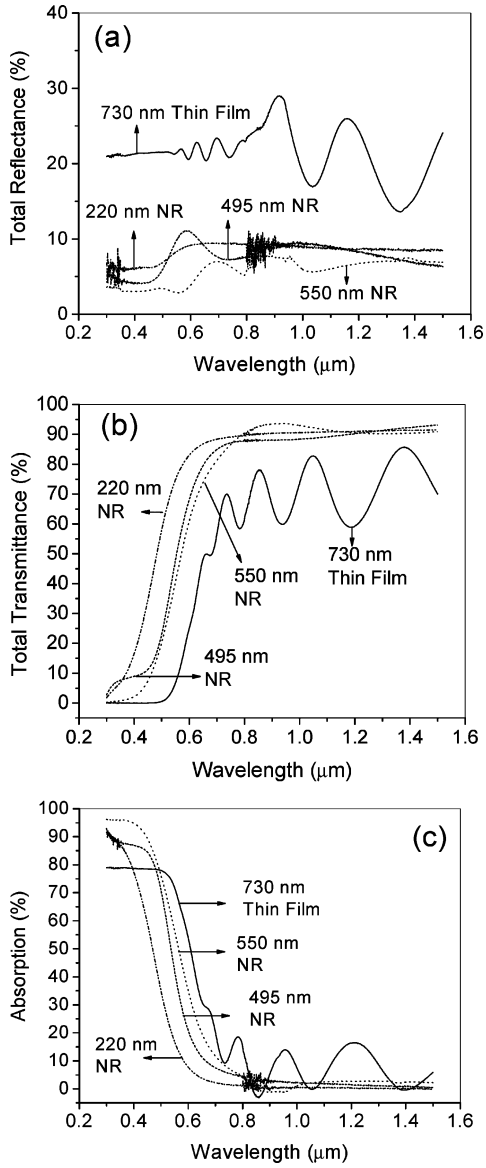

Figure 2. Results of (a) reflectance (*R*), (b) transmittance (*T*), and (c) percentage absorption ($A = 1 - R - T$) measurements for In_2S_3 thin film (thickness $t = 730$ nm) and nanorod (NR) samples (length $l = 220, 495, 550$ nm) over a wavelength of $\lambda = 0.3-1.5$ μm.

tance (at a given wavelength) is not linearly proportional to the nanorod length and suggests that there is a possibility of enhanced absorption due to the other effects. In fact, the very low reflectance values of nanorods (Figure 2a) indicate that a nanostructured layer leads to a noticeable gain in the absorption (Figure 2c). The absorption values increase to approximately 96% for 550 nm long nanorods at wavelengths shorter than 500 nm. The absorption of shorter nanorod samples is also in the vicinity of the relatively high value of 90% at wavelengths shorter than 400 nm. Despite its much larger thickness (730 nm) and high mass density as opposed to the porous (~31%) and shorter nanorod samples, the absorption of the conventional thin film indium sulfide was only approximately 79%. This is a significant enhancement in the optical absorption, which can lead to superior photovoltaic and photoconductive properties.

In previously reported studies for columnar thin films, high absorption values were observed and were attributed to possible oxidation on the surface.[35] In comparable studies on indium sulfide and copper indium sulfide, high optical absorption was also correlated with oxidation effects.[20,23] However, EDAX analysis performed on our samples showed the amount of oxygen on the surface of indium sulfide nanorods was about 0.20 ± 0.05%. Other possible effects responsible for enhanced absorption are grain size, quantum size effects, and high density of dislocations in the film structure.[36] Our X-ray diffraction (XRD) analysis showed no diffraction peaks, indicating an amorphous structure, which eliminates possible crystal-structure-related effects.[15] Partial quantum size effects might take place since the SEM results indicate a highly rough and cauliflower-like formation on individual rods, which may introduce finer nanostructures with sizes smaller than 5−10 nm and thus bring about quantum effects.

We believe that the significant increase observed in the optical absorption of nanorods is mainly due to "random light scattering" taking place within the nanorod layer, the increased pathway of light, and thus maximized chance for the absorption of light. The contribution of random scattering effects in low reflectance materials was previously studied in the literature.[28,37] Contrary to the thin film (see Figure 1a,b), SEM images of nanorod samples (see Figure 1c,d) indicate extremely rough and random surface patterns, thus leading to a significant "diffuse light scattering" process taking place within the nanorod morphology. The reflectance (Figure 3a), transmission (Figure 2b), and absorption (Figure 2c) profiles show a trend following the nanorod length; yet, even for the shortest 220 nm long nanorods, absorption is drastically higher than for the much thicker and denser thin films, despite the 31% porosity of the nanorod layers.

In order to investigate the scattering phenomena in the nanorods in more detail, we performed measurements of diffuse and specular components of the transmitted and reflected light (Figure 3a,b, respectively) from the 495 nm long nanorod samples. In Figure 3a, the diffuse transmittance component values at shorter wavelengths (<500 nm), where high absorption is observed (~96%, see Figure 2c), are comparable to the specular component and constitutes about 50% or more of the transmittance. It reduces to a fraction of the specular component at longer wavelengths. For reflectance, the diffuse component becomes a much larger contributor than the specular component at wavelengths shorter than 500 nm. Almost 90% of the total reflected light belongs to diffuse components at the region where we also observed high absorption. The significant contribution of the diffuse components of reflected and transmitted light from the nanorods is

indicative of strong random scattering within and on the surface of the nanorod morphology. The overlap of enhanced scattering and absorption spectra is supportive of the random scattering effect in the increased absorption that we observe. The angular dependence of reflectance on both incidence and radiation patterns, as well as the polarization dependence, has not been performed for our samples, but a theoretical analysis in relation to the light scattering on highly rough nanorod surfaces together with further detailed analysis is currently being performed.

For a preliminary theoretical concept, we have applied the Shirley−George (SG) model[38] for strong diffusers on our nanorod array geometry. In this model, two types of surfaces, conical and paraboloidal depending on the shape of the autocorrelation function near the origin, are analyzed and their angular radiation patterns are calculated. For the conical profile, the autocorrelation function is cone-shaped near the origin, and the reflectance pattern depends on

$$q = \frac{\omega}{\lambda S^2} \quad (1)$$

where ω is the correlation length of surface roughness, λ is the wavelength, and S is the rms phase delay. This pattern is observed in surfaces with high slopes and discontinuities, which conceptually fit our nanorod samples[38] (see Figure 1c,d). For a paraboloidal surface, the autocorrelation function is paraboloidal near the origin, and the reflectance pattern is related to $q = \omega/\lambda S$. For $q \ll 1$, strong diffuser conditions are expected for both kinds of surfaces. The SG model is applicable to both reflecting and transmitting surfaces that introduce a diffuse scattering of the incident light beam.[38] For the reflectors, a strong diffuser rms phase delay S satisfies the relation

$$S = 4\pi\frac{\sigma_h}{\lambda}\cos(\theta_0) \gg 1 \quad (2)$$

where σ_h is the rms diffuser height and θ_0 is the angle of incidence for incoming light.

In a conical diffuser, the angular distribution of reflectance for a normal incidence angle light ($\theta_0 = 0$) is given by

$$I_n = \cos\theta\, 2\pi\left(\frac{\omega}{\lambda S^2}\right)\left\{1 + \left(\frac{2\pi\omega}{\lambda S^2}\right)^2(\sin^2\theta)\right\}^{-3/2} \quad (3)$$

or from eq 1

$$I_n = \cos\theta\, 2\pi q\{1 + (2\pi q)^2(\sin^2\theta)\}^{-3/2} \quad (4)$$

where θ is the angle of the scattered light. Since the SG model can be used to obtain the angular distribution of scattering, it can provide an insight about the intensity of random scattering taking place on the surface.

In the case of indium sulfide nanorod arrays, when the angle of incidence is $\theta_0 = 0$ (*i.e.*, normal incident light), using eqs 1 and 2, q can be written as

$$q = \frac{\omega\lambda}{(2\pi\sigma_h)^2} \quad (5)$$

Approximating the rms height, σ_h, by the value of the GLAD nanorods (*i.e.*, $\sigma_h \approx$ 220, 495, and 550 nm) and the average correlation length, ω, by the value of average nanorod diameter (*i.e.*, $\omega \approx$ 100 nm), eq 5 gives a q value well below 1 for the visible spectrum of light, thus indicating our nanorods are in the strong diffuser category.

In Figure 4a, the reflectance *versus* angular distribution pattern for various q values is plotted using eq 4. From eq 1, q is proportional to ω and inversely related to σ_h. As also can be seen in Figure 4a, by decreasing q (*e.g.*, for a very rough surface with large rms height σ_h and small correlation length ω), the integrated reflected intensity decreases significantly (note the logarithmic scale in *y*-axis of Figure 4a) and the angular distribution approaches a more uniform shape, in this case, a Lambertian diffuser. The SG model is focused on the portion of the light that is reflected from the surface, by which it can be assumed that the rest of the light is either transmitted or absorbed by the material. Therefore, a reduced integrated reflectance intensity indicates that the amount of absorbed and/or transmitted light is enhanced. On the basis of the SG model, as the lengths of our GLAD nanorods increase (*i.e.*, larger σ_h) and, therefore, the q value decreases, a more uniform angular distribution in diffuse component of the reflected light and reduced integrated reflectance intensity are predicted, consistent with our experimental results. Also based on the SG model, an increased amount of light that was not reflected due to the rough morphology of our GLAD nanorods

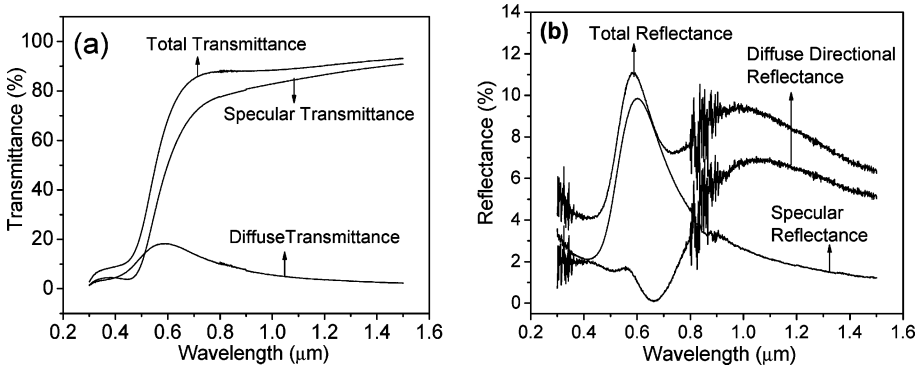

Figure 3. Specular and diffuse components of (a) transmittance and (b) reflectance profiles measured for 495 nm long indium sulfide nanorod (NR) sample over a wavelength of λ = 300−1500 nm.

would be captured inside the nanorod layer, which would be transferred to the lower parts enhancing the penetration length and thus the chances of absorption compared to within a flat thin film. Moreover, enhanced diffuse scattering of light is also expected to contribute to the random scattering process among the side walls of the nanorods, which can lead to further enhancement in light absorption. In addition, the λ dependence in eq 3 results in a decrease in q values for shorter wavelengths and, therefore, increased diffuser strength. This is consistent with enhanced diffuse scattering of light from a rough surface with feature sizes smaller than the wavelength.[37] Therefore, according to the mechanism explained above in the SG model, diffuse scattering and absorption of light are expected to be further enhanced for our GLAD nanorods at shorter wavelength, also consistent with our experimental results.

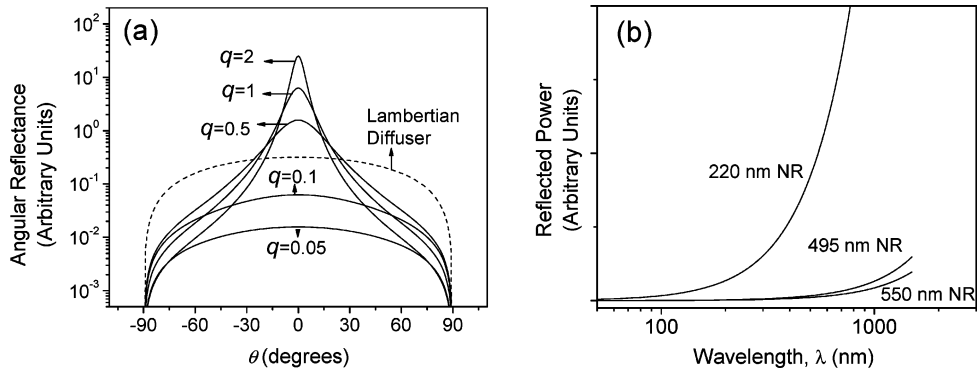

Figure 4. (a) Angular reflectance for various values of $q = \omega\lambda/(2\pi\sigma_h)^2$, and (b) estimated reflected power (integrated total reflectance from eq 6) for different values of nanorod (NR) length.

From eq 3, we can also analyze the total integrated intensity of the reflected light for a normally incident beam. Integrating eq 3 through $-90° < \theta < 90°$, the total reflected power can be calculated as

$$P = \left[1 + \left(\frac{2\pi\omega}{\lambda S^2}\right)^2\right]^{-1/2} \quad (5)$$

Replacing the S value by its original form in eq 2

$$P = \left[1 + \left(\frac{\omega\lambda}{8\pi\sigma_h^2}\right)^2\right]^{-1/2} \quad (6)$$

which is λ dependent. Using eq 6, in Figure 4b, we plot the total reflected power *versus* wavelength curves for samples of different nanorod lengths with the approximation $\sigma_h \sim$ nanorod length. We note that the total integrated reflection over the hemisphere of incidence is calculated also including the specular reflection. In these plots, the correlation length, ω, of nanorods is approximated by the average nanorod diameter, ~100 nm, and the spectrum of λ covers from 50 to 2000 nm. It is clear from Figure 4b that, by decreasing λ, the total integrated reflected power is also decreased. This asserts that, by increased diffuser strength, total reflected power decreases. In turn, the rest of the incident power (*i.e.*, light) is either transmitted through the media or absorbed by the material. For the case of GLAD nanorods, this translates into a higher amount of light trapped inside the nanostructured layer, which increases the overall absorption rate compared to within a flat thin film. In addition, light that is passing through the nanorod layer can go through random scattering events, travel a longer pathway inside, and therefore have a better chance of being absorbed. In other words, besides the well-known effects of band gap and thickness of the nanorod layer, light absorption in GLAD nanorods is expected to be proportional to the amount of light that is not being reflected. Therefore, the more diffused the light is, the more likelihood there is redirection of the light toward the material, and the more absorption can occur.

The results of Figure 4a,b also agree with our experimental results shown in Figure 2. In Figure 2a, the total reflectance *versus* wavelength is decreased by increasing the nanorod length which corresponds with the plots in Figure 4a, wherein the reflected intensity envelope is shifted down by increasing the diffuser strength. Similarly in Figure 2c, a shift of absorption thresholds toward longer wavelengths by increasing nanorod length coincides well with the results shown in Figure 4b, where the decrease of total reflected power (higher absorption or transmission) is associated with increased nanorod length.

For the proof-of-concept photoconductivity (PC) tests, indium sulfide nanorods were deposited by GLAD onto commercial ITO-on-glass samples using the same conditions as described above. Conventional thin film indium sulfide samples were prepared using normal incidence deposition. Resistance measurements for the PC tests were performed by an Agilent 34410 digital sourcemeter unit using two probes. The sample size was 8 cm^2 for nanorod and thin film samples. The nanorod sample was coated with a silver thin film using a GLAD capping process through an aluminum mask with circular openings of 0.3 cm^2. The GLAD capping was performed by sputter depositing silver onto indium sulfide nanorods starting with an 85° angle and gradually changing the deposition angle to normal incidence. The thickness of the silver capping layer was measured to be approximately 2 μm. By this method, a resistor was formed between the ITO contact layer and the silver capping layer for PC measurements. The thin film indium sulfide samples and bare ITO samples were also coated with silver using normal incidence sputter deposition through circular masks. ITO substrates directly

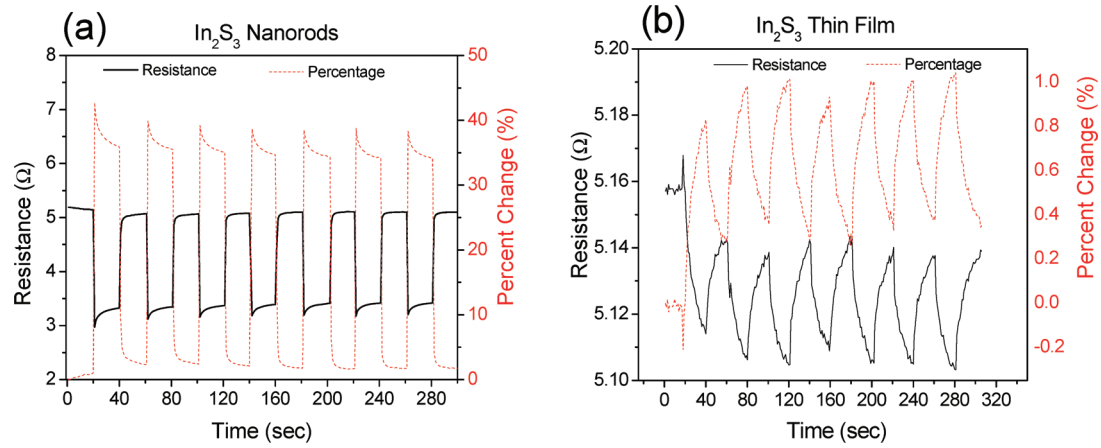

Figure 5. Resistance and percent change in resistance plots are shown for photoconductive (PC) device samples of indium sulfide (a) nanorods and (b) thin film structures as a function of time. Light source is turned on and off during PC experiments, and resistance of samples decreases (*i.e.*, PC increases) when the light is switched on.

coated with silver were used to obtain the resistance of the system excluding the indium sulfide layer (*i.e.*, total resistance of the ITO layer and contact resistance due to the probe−silver interface). This background resistance was measured to be about 4.8Ω. PC measurements were performed by measuring the total resistance of the system including indium sulfide resistance and background resistance. The PC response of indium sulfide was calculated by subtracting the background resistance from the total resistance. The resistance *versus* time curves are shown in Figure 5. The light source (465 nm monochromatic light) was switched on and off with 20 s intervals. As seen in Figure 5a, PC *versus* time curve for the nanorod sample shows up to about 40% decrease in resistance when the light is on. On the other hand, the resistance change observed in the conventional indium sulfide thin film of Figure 5b, under identical conditions, is less than 1%. Additionally, the resistance of nanorods stabilizes in a short time, where the thin film sample shows less stability and drifts over time. This preliminary photoconductivity result shows the potentially superior photoconductive response of our nanorods, which is believed to be due to enhanced light absorption, as observed in our optical measurements above.

CONCLUSION

In conclusion, we fabricated indium sulfide nanorod arrays and thin films of various thicknesses using GLAD thermal evaporation. Detailed optical measurements on the samples were performed for reflectance, transmittance, and absorption using an integrating sphere. Results showed that indium sulfide nanorod layers have significantly lower reflectance and superior optical absorption values compared to conventional flat indium sulfide thin films. We observed that, by controlling the length of the nanorods, it is possible to obtain absorption values as high as 90−96%, especially at wavelengths shorter than 500 nm. Our detailed analysis on optical measurements and a theoretical study based on the Shirley−George model for strong diffusers indicate that enhanced optical absorption in nanorods can originate from trapping of light and random scattering process occurring within the extremely rough nanorod layer. In addition, enhanced absorption in nanorods was observed to lead to a superior photoconductivity response, while the conventional thin film of indium sulfide showed an insignificantly low photoconductivity change. These observations point to the usefulness of nanostructured materials in developing high efficiency solar cell and photodetector applications for a wide range of photosensitive materials. We plan to further expand our study on detailed photoconductivity and photovoltaic tests on indium sulfide, as well as for other materials of interest. A more detailed theoretical analysis of the high optical absorption observed in GLAD-deposited nanorods is also in process.

METHODS

We deposited arrays of indium sulfide nanorods in a custom-designed vacuum thermal evaporation GLAD system on silicon (100) wafers, glass, and indium tin oxide (ITO) substrates. The minimum size of the samples was 1 in. × 1 in. as required by our optical measurements. The source material used was 99.99% purity In_2S_3 in powder form from CERAC. Depositions were carried out at room temperature under 7.5×10^{-6} Torr base pressure. We used a carbon crucible with a resistive tungsten basket heater for evaporation. Since In_2S_3 is quite challenging to evaporate steadily due to flash explosions because of the large sulfur vapor pressure, the crucible was heated to the evaporation temperature gradually. Until a stable evaporation rate was reached, deposition onto substrate surface was avoided by a shutter. The evaporation rate was monitored using a Sigma Instruments Q-pod QCM monitor placed at a 45° angle toward the evaporation basket and was kept at a stable value of 2 nm/s. Depositions were carried out at an 85° incidence angle measured between

the incident flux and the substrate normal. In addition, the sample was uniformly rotated around the substrate normal axis at a speed of 1 rpm.

We prepared indium sulfide nanorod samples of three different lengths (220, 495, and 550 nm) and thin films with a thickness of 730 nm on Si(100), ITO, and glass substrates. Nanorod and thin film coatings on glass substrates are used for optical reflectance, transmission, and absorption measurements.

The morphology and chemical composition of the samples were measured by scanning electron microscopy (SEM) (JEOL 7000F) and energy-dispersive X-ray analysis (EDAX), respectively. Optical absorption, reflectance, and transmittance data were obtained in the laboratories of Surface Optics Corporation (SOC) by using a UV−vis spectrophotometer incorporating an integrating hemisphere. During optical measurements, wavelengths of light ranged from 300 to 1500 nm, and the incident angle of the beam was 8°.

Photoconductivity (PC) experiments were performed by illuminating the thin film and nanorod samples using a 465 nm LED source at normal incidence with 15 kcd/m^2 luminosity. The thickness of the nanorod samples was 495 nm and the thin film was 730 nm.

Acknowledgment. This work was supported by a NASA/Arkansas EPSCoR Research Infrastructure Development grant administered through the Arkansas Space Grant Consortium, and by matching funds from the University of Arkansas—Little Rock and Arkansas State University. The authors would also like to thank the UALR Nanotechnology Center staff for their assistance in SEM and XRD measurements.

REFERENCES AND NOTES

1. Kim, W.-T.; Lee, W.-S.; Chung, C.-S.; Kim, C.-D. Optical Properties Of In_2S_3: Co(2+) Single Crystals. *J. Appl. Phys.* **1988**, *63*, 5472–5475.
2. Govender, K.; O'Brien, P.; Smyth-Boyle, D. Improved Routes towards Solution Deposition of Indium Sulfide Thin Films for Photovoltaic Applications. *Mater. Res. Soc. Symp. Proc.* **2002**, *692*, 525–530.
3. Mathew, M.; Sudha Kartha, C.; Vijayakumar, K. P. *Advances in Energy Research* **2006**, 217–221.
4. Amlouk, M.; Ben Said, M. A.; Kamoun, N.; Belgacem, S.; Brunet, N.; Barjon, D. Acoustic Properties of β-In_2S_3 Thin Films Prepared by Spray. *Jpn. J. Appl. Phys., Part 1* **1999**, *38*, 26–30.
5. O'Brien, P.; Octway, D. J.; Walsh, J. R. Novel Precursors for the Growth of α-In_2S_3: Trisdialkylthiocarbamates of Indium. *Thin Solid Films* **1998**, *315*, 57–61.
6. Pathana, H. M.; Lokhandea, C. D.; Kulkarnia, S. S.; Amalnerkarb, D. P.; Sethb, T.; Sung-Hwan, H. Some Studies on Successive Ionic Layer Adsorption and Reaction (Silar) Grown Indium Sulphide Thin Films. *Mater. Res. Bull.* **2005**, *40*, 1018–1023.
7. Yoosuf, R.; Jayaraj, M. K. Optical and Photoelectrical Properties of β-In_2S_3 Thin Films Prepared by Two-Stage Process. *Sol. Energy Mater. Sol. Cells* **2005**, *89*, 85–94.
8. Rehwald, W.; Harbeke, G. On the Conduction Mechanism in Single Crystal β-Indium Sulfide In_2S_3. *J. Phys. Chem. Solid* **1965**, *26*, 1309–1318.
9. Diehl, R.; Nitsche, R. Vapour Growth of Three In_2S_3 Modifications by Iodine Transport. *J. Cryst. Growth* **1975**, *28*, 306–310.
10. Allsop, N. A.; Schönmann, A.; Belaidi, A.; Muffler, H. J.; Mertesacker, B.; Bohne, W.; Strub, E.; Röhrich, J.; Lux-Steiner, M. C.; Fischer, Ch.-H. Indium Sulfide Thin Films Deposited by the Spray Ion Layer Gas Reaction Technique. *Thin Solid Films* **2006**, *513*, 52–56.
11. Barreau, N.; Mokrani, A.; Couzinié-Devy, F.; Kessler, J. Bandgap Properties of the Indium Sulfide Thin-Films Grown by Co-Evaporation. *Thin Solid Films* **2009**, *517*, 2316–2319.
12. Timoumi, A.; Bouzouita, H.; Brini, R.; Kanzari, M.; Rezig, B. Optimization of Annealing Conditions of In_2S_3 Thin Films Deposited by Vacuum Thermal Evaporation. *Appl. Surf. Sci.* **2006**, *253*, 306–310.
13. Bouabid, K.; Ihlal, A.; Outzourhit, A.; Ameziane, E. L. Structural and Optical Properties of In_2S_3 Thin Films Prepared by Flash Evaporation. *Act. Passive Electron. Compon.* **2004**, *27*, 207–214.
14. John, T T.; Sudha Kartha, C.; Vijayakumar, K. P.; Abe, T.; Kashiwaba, Y. Preparation of Indium Sulfide Thin Films by Spray Pyrolysis Using a New Precursor Indium Nitrate. *Appl. Surf. Sci.* **2005**, *252*, 1360–1367.
15. Kumar, P. M. R.; John, T. T.; Kartha, C. S.; Vijayakumar, K. P.; Abe, T.; Kashiwaba, Y. Effects of Thickness and Post Deposition Annealing on the Properties of Evaporated In_2S_3 Thin Films. *J. Mater. Sci.* **2006**, *41*, 5519–5525.
16. Barreau, N.; Marsillac, S.; Bernède, J. C.; Barreau, A. Investigation of β-In_2S_3 Growth on Different Transparent Conductive Oxides. *Appl. Surf. Sci.* **2000**, *161*, 20–26.
17. Naghavi, N.; Spiering, S.; Powalla, M.; Cavana, B.; Lincot, D. High-Efficiency Copper Indium Gallium Diselenide (CIGS) Solar Cells with Indium Sulfide Buffer Layers Deposited by Atomic Layer Chemical Vapor Deposition (ALCVD). *Prog. Photovoltaics* **2003**, *11*, 437–443.
18. Hariskos, D.; Ruckh, M.; Rühle, U.; Walter, T.; Schock, H. W.; Hedström, J.; Stolt, L. A Novel Cadmium Free Buffer Layer for Cu(In,Ga)Se_2. *Sol. Energy Mater. Sol. Cells* **1996**, *41/42*, 345–353.
19. Nakada, T.; Mizutani, M. 18% Efficiency Cd-Free Cu(In,Ga)Se_2 Thin-Film Solar Cells Fabricated Using Chemical Bath Deposition (CBD)-ZnS Buffer Layers. *Jpn. J. Appl. Phys., Part 2* **2002**, *41*, L165–L167.
20. Barreau, N.; Bernède, J. C.; El Maliki, H.; Marsillac, S.; Castel, X.; Pinel, J. Recent Studies on In_2S_3 Containing Oxygen Thin Films. *Solid State Commun.* **2002**, *122*, 445–450.
21. Liang, C.; Shimizu, Y.; Sasaki, T.; Umehara, H.; Koshizaki, N. One-Step Growth of Silica Nanotubes and Simultaneous Filling with Indium Sulfide Nanorods. *J. Mater. Chem.* **2004**, *14*, 248–252.
22. Rao, R.; Chandrasekaran, H.; Gubbala, S.; Sunkara, M. K.; Daraio, C.; Jin, S.; Rao, A. M. Synthesis of Low-Melting Metal Oxide and Sulfide Nanowires and Nanobelts. *J. Electron. Mater.* **2006**, *35*, 941–946.
23. Akkari, C. F.; Brini, R.; Kanzari, M.; Rezig, B. High Absorbing $CuInS_2$ Thin Films Growing by Oblique Angle Incidence Deposition in Presence of Thermal Gradient. *J. Mater. Sci.* **2005**, *40*, 5751–5755.
24. Patra, C. R.; Patra, S.; Gabashvili, A.; Mastai, Y.; Koltypin, Y.; Gedanken, A.; Palchik, V.; Slifkin, M. I. A Microwave Route for the Synthesis of Nanoflakes and Dendrites-Type β-In_2S_3 and Their Characterization. *J. Nanosci. Nanotechnol.* **2006**, *6*, 845–851.
25. Zhao, P.; Huang, T.; Huang, K. Fabrication of Indium Sulfide Hollow Spheres and Their Conversion to Indium Oxide Hollow Spheres Consisting of Multipore Nanoflakes. *J. Phys. Chem. C* **2007**, *111*, 12890–12897.
26. Vick, D.; Brett, M. J. Conduction Anisotropy in Porous Thin Films with Chevron Microstructures. *J. Vac. Sci. Technol., A* **2006**, *24*, 156–164.
27. Michijima, M.; Hayashi, H.; Kyoho, M.; Nakabayashi, T.; Komoda, T.; Kira, T. Oblique-Incidence Anisotropy in Very Thin Ni-Fe Films. *IEEE Trans. Magn.* **1999**, *35*, 3442–3444.
28. Yang, Z. P.; Ci, L.; Bur, J. A.; Lin, S. Y.; Ajayan, P. M. Experimental Observation of an Extremely Dark Material Made by a Low-Density Nanotube Array. *Nano Lett.* **2008**, *8*, 446–451.
29. Kanamori, Y.; Hane, K.; Sai, K.; Yugami, H. 100 nm Period Silicon Antireflection Structures Fabricated Using a Porous Alumina Membrane Mask. *Appl. Phys. Lett.* **2001**, *78*, 142.
30. Sun, C.; Jiang, P.; Jiang, B. Broadband Moth-Eye Antireflection Coatings on Silicon. *Appl. Phys. Lett.* **2008**, *92*, 061112.
31. Koynov, S.; Brandt, M.; Stutzmann, M. Black Nonreflecting Silicon Surfaces for Solar Cells. *Appl. Phys. Lett.* **2006**, *88*, 203107.1203107.3.
32. Xi, Q.; Schubert, M. F.; Kim, J. K.; Schubert, E. F.; Chen, M.; Lin, S.-Y.; Liu, W.; Smart, J. A. Optical Thin-Film Materials with Low Refractive Index for Broadband Elimination of Fresnel Reflection. *Nat. Photonics* **2007**, *1*, 176–179.

33. Xi, J.-Q.; Kim, J. K.; Schubert, E. F.; Ye, D.; Lu, T.-M.; Lin, S.-Y.; Juneja, J. S. Very Low-Refractive-Index Optical Thin Films Consisting of an Array of SiO_2 Nanorods. *Opt. Lett.* **2006**, *31*, 601–603.
34. Lee, Y.-J.; Ruby, D. S.; Peters, D. W.; McKenzie, B B.; Hsu, J. W. P. Optical Absorption Enhancement in Amorphous Silicon Nanowire and Nanocone Arrays. *Nano Lett* **2008**, *8*, 1501–1505.
35. Kivaisi, R. T. Optical Properties of Obliquely Evaporated Aluminum Films. *Thin Solid Films* **1982**, *97*, 153–163.
36. Tyagi, P. J.; Vedeshwar, A. G. Grain Size Dependent Optical Band Gap of CdI_2 Films. *Bull. Mater. Sci.* **2001**, *24*, 297.
37. Sterligov, V. A.; Cheyssaca, P.; Blau, W.; Kröll, M. Scattering and Reflective Properties of a Hexagonal Lattice Of Nanorods. *Opt. Commun.* **2003**, *226*, 125–134.
38. Shirley, L. G.; George, N. Diffuser Radiation Patterns over a Large Dynamic Range. Part 1: Strong Diffusers. *Appl. Opt.* **1988**, *27*, 1850–1861.